



LAWRENCE
LIVERMORE
NATIONAL
LABORATORY

Spinodal Decomposition and Ordering Transformation in U-6 wt% Nb

L. L. M. Hsiung

August 17, 2005

Solid- Solid Phase Transformations in Inorganic Materials
2005

Phoenix, AZ, United States

May 29, 2005 through June 3, 2005

Disclaimer

This document was prepared as an account of work sponsored by an agency of the United States Government. Neither the United States Government nor the University of California nor any of their employees, makes any warranty, express or implied, or assumes any legal liability or responsibility for the accuracy, completeness, or usefulness of any information, apparatus, product, or process disclosed, or represents that its use would not infringe privately owned rights. Reference herein to any specific commercial product, process, or service by trade name, trademark, manufacturer, or otherwise, does not necessarily constitute or imply its endorsement, recommendation, or favoring by the United States Government or the University of California. The views and opinions of authors expressed herein do not necessarily state or reflect those of the United States Government or the University of California, and shall not be used for advertising or product endorsement purposes.

SPINODAL DECOMPOSITION AND ORDERING TRANSFORMATION IN U-6 wt% Nb

Luke L. M. Hsiung

Lawrence Livermore National Laboratory
Chemistry and Materials Science Directorate
P.O. Box 808, L-352
Livermore, CA 94551-9900

Abstract

Phase stability and aging mechanisms in a water-quenched (WQ) U-6wt% Nb (WQ-U6Nb) alloy artificially aged at 200°C (16 hours) and naturally aged at room temperature for 15 years have been investigated. Age hardening/softening phenomenon is recorded from the artificially aged samples by microhardness measurement. The age hardening can be readily rationalized by the occurrence of spinodal decomposition (or fine-scaled Nb segregation), which results in the formation of a modulated structure in the aged samples. Prolonged aging leads to age softening of the alloy by coarsening of the modulated structure. Disorder-order or chemical ordering transformation is found within the naturally aged alloy according to TEM observations of antiphase domain boundaries (APBs) and superlattice diffraction patterns. The formation of a partially ordered phase in the naturally aged alloy is proposed and identified.

Introduction

It is well known that U-6wt. %Nb (U-14 at. %Nb) alloy as exploited for a variety of engineering applications has a microstructure containing martensitic phases supersaturated with Nb, which can be obtained by rapid quenching the alloy from γ (bcc)-field solid solution to room temperature [1, 2]. The high cooling rate forces the γ -phase solid solution to transform martensitically to a variant of the low temperature α (orthorhombic) phase in which Nb is retained in supersaturated solid solution. Because the variant phase is supersaturated and its lattice parameters differ from the equilibrium α phase, it has been designated α' martensite. Two additional variant phases, a monoclinic distortion of α' , named α'' martensite, or a tetragonal distortion of γ , named γ^o martensite, can also be formed within the as-quenched material. The resulting alloy has improved mechanical properties (ductility and toughness) and excellent corrosion resistance because of the uniform distribution of Nb in solid solution that suppresses the diffusional decomposition reaction to form two-phase (an α phase and a Nb-enriched γ phase) cellular microstructures, which are undesirable for engineering applications.

It has been reported that the water-quenched (WQ) U6Nb alloy containing extensively twinned α'' martensitic microstructure results in low yield strength (~200 MPa) and high tensile ductility (~30%) [2]. It has also been demonstrated that the U-Nb alloy containing α'' martensite reveals shape memory effect [3], and the shape memory behavior is controlled mainly by the twin structures within the alloy [4]. Aging of the α'' martensite in the 150°C to 400°C range results in increase of yield strength to as high as 1.3 GPa due to very fine scale microstructural changes [5], which have not yet been fully

characterized but may have involved spinodal decomposition. Over-aging occurs at temperatures above 400°C, where cellular decomposition occurs to form coarse two-phase cellular microstructures. The occurrence of these decompositions in association with Nb segregation can subsequently deteriorate and embrittle the alloys by reducing ductility and toughness as well as corrosion resistance [2, 5]. Therefore, it is necessary to investigate and understand the aging effects on the microstructural and phase stability of WQ-U6Nb alloy. The investigation of aging effects on WQ-U6Nb reported in the open literature up to present has mainly been placed on aging at temperatures above 400°C. Relatively little is known about the aging mechanism of WQ-U6Nb below 400°C, a detailed investigation of segregation reaction within isothermally aged WQ-U6Nb below 400°C was previously reported by Beverini and Edmonds [6], who investigated the low-temperature aging behavior using Vickers hardness measurement and Atom Probe Field Ion Microscopy (APFIM) methods. According to their report, an age hardening/softening phenomenon associated with nanometer length-scale of segregation reaction, possibly spinodal decomposition, was detected within the aged alloy samples. It is noted that the spinodal decomposition is a continuous clustering mechanism in which the supersaturated solid solution separates spontaneously into solute-lean and solute-rich phases within the parent phase domain through uphill diffusion, which is totally different from the nucleation and growth mechanism via downhill diffusion [7]. In order to further elucidate the low-temperature aging mechanisms, our investigation was accordingly focused on the phase stability of the WQ-U6Nb alloy during isothermal aging below 200°C.

Experimental

The U6Nb alloy used for this investigation was wrought processed from Rocky Flats VAR VAR ingot at the BWXT/Bechtel Y-12 plant. Detailed information regarding the fabrication process can be found in [2]. Nb contents (in wt%) analyzed from different locations of the ingot were 5.79 (bottom edge), 5.97 (top edge), 6.03 (bottom center), and 6.10 (Top center). Five rod-shape samples of 3 mm in diameter were machined from a wrought-processed 38 mm thick plate. Each of these five samples was then encapsulated in a Cu tube and was solution treated at 800°C for 4 hours followed by water quench. One of the water-quenched samples was examined and characterized under as water-quenched condition (designated as WQ). The remaining four of the water-quenched samples were isothermally aged at 200°C for 2 hours (designated as 2h), 4 hours (4h), 8 hours (8h), and 16 hours (16h). Sample NA was designated to a naturally aged sample obtained from a 15-year old alloy sample. X-ray diffraction analysis was conducted with all the samples using a Philips XRG diffractometer with Cu ($K\alpha$) radiation ($\lambda = 1.5406\text{\AA}$). The employed scanning angles (2θ) for diffraction ranged from 20° to 80° with a scanning rate of 2° min⁻¹. Microhardness measurements were performed on all these samples using a Vickers-hardness indenter. The applied load was 50 g and the time duration is 35 sec for each test. To obtain a statistically significant value, six tests were conducted for each measurement. Microstructures of the WQ, the artificially aged, and the NA samples were examined using a JEOL 200CX transmission electron microscope (TEM). TEM foils were machined from the rod-shape samples and the final thinning of the foils was prepared by twinjet electropolishing in a solution of 45 vol% methanol, 45 vol% butyl alcohol and 10 vol% nitric acid at 50 V and -20°C.

Results and Discussion

Artificial aging at 200°C

Figure 1 shows the results obtained from Vickers-hardness measurement of the WQ-U6Nb and isothermally aged at 200°C, in which a significant change in hardness can be readily seen. The hardness initially increases from HV 190.0 ± 5.8 for the WQ sample to HV 237.0 ± 6.4 and 254.8 ± 12.2 for the 4h and 8h samples respectively and then decreases to HV 237.3 ± 10.0 for the 16h sample. The age hardening/softening phenomenon observed in Fig. 1 is consistent with the result reported previously in [6]. It is noted that the change of phase content and microstructural morphology of the artificially aged samples is insignificant. The hardening/softening phenomenon can be better interpreted by the occurrence of spinodal decomposition resulted from short-range diffusion, which leads to the formation of a modulated structure shown in Figs. 2(a) – 2(d). It is noted that the fine-scale modulated structure caused by spinodal decomposition generally appeared as dark/bright fringes in TEM image accompanied by the appearance of satellite (or side) spots around the Bragg spots of the diffraction pattern [8,9]. A modulated structure, which presumably contains very fine domains (~ 3 nm in size) of Nb-lean and Nb-rich phases resulted from spinodal decomposition, was first observed at a local region within the 2h sample [Fig. 2(a)]. It became more pronounced and to cover a larger portion of the 4h and 8h sample [Figs. 2(b) and (c)], which causes the hardness to increase to a maximum. Further aging causes the coarsening of the modulated structure to occur, which subsequently leads to a decrease in hardness. As can be clearly seen in Fig. 2(d), an increase of domain width to ~ 50 nm was observed within the 16h sample. Since the change of segregated phase-domains can affect the mobility of dislocation motion during deformation, it influences the hardness (strength) of artificially aged samples. In summary, we have so far revealed the formation of nano-scale modulated structure within the artificially aged alloy samples. The forming and coarsening of modulated domains result in the occurrence of age hardening/softening behavior according to the microhardness measurement.

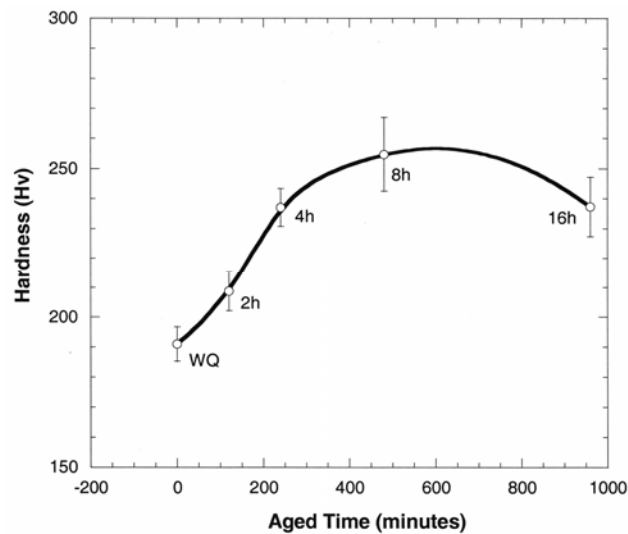


Fig. 1. Results of microhardness measurement showing the age hardening/softening behavior of the WQ-U6Nb alloy isothermally aged at 200°C.

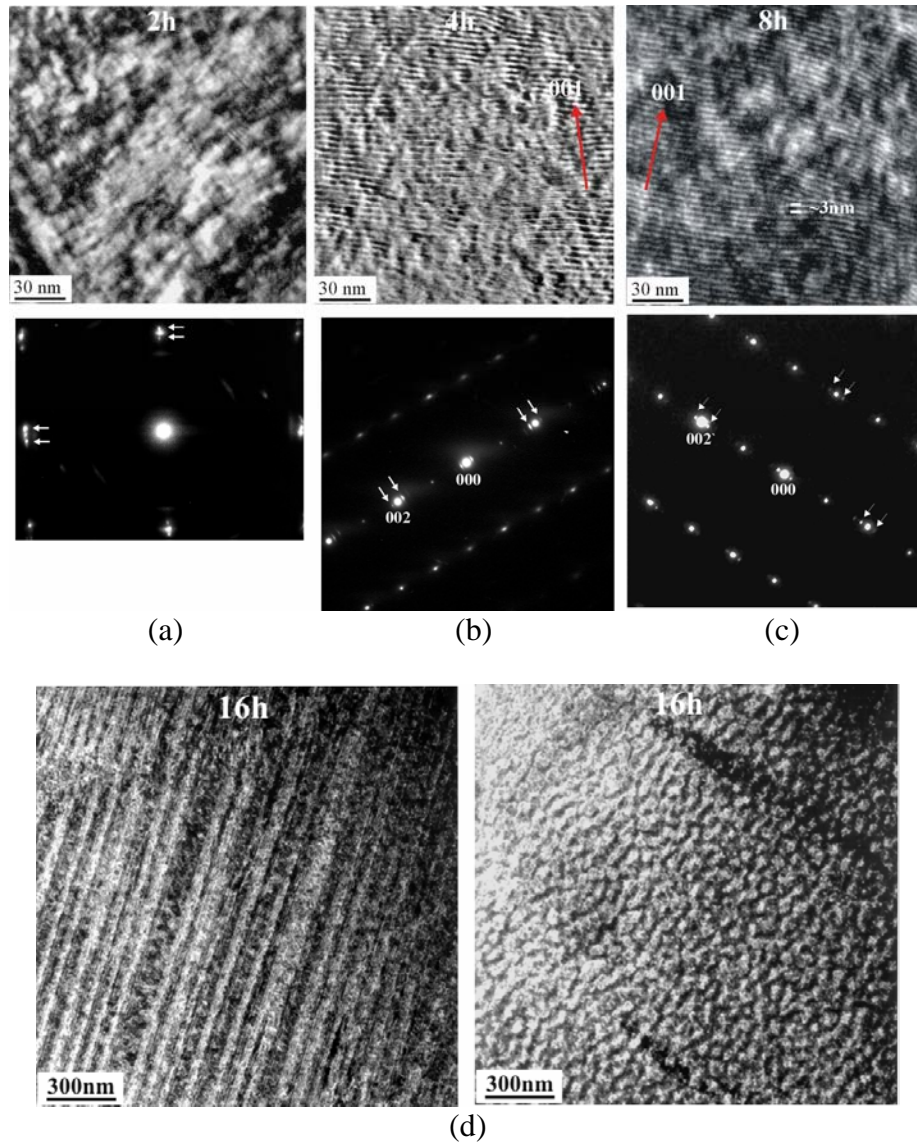


Fig. 2. TEM images and selected-area diffraction (SAD) patterns showing the formation of modulated structures within the artificially aged 2h, 4h, 8h and 16h samples. Satellite (Side) spots caused by the modulation are arrowed in SAD patterns shown in (a), (b), and (c). Coarsening of the modulation observed in 16h sample is shown in (d).

Natural aging at room temperature

Similar to the artificially aged samples, the change of microstructural morphology within the 15-year NA sample is insignificantly noticeable. However, a very interesting finding within the NA sample is the formation of swirl-shape antiphase domain boundaries (APBs) as shown in Fig. 3. It is worthy to note that the contrast of antiphase domain boundary (also known as π boundary) is visible when the phase angle $\alpha = 2\pi\mathbf{g}\cdot\mathbf{P} = \pi$ and is invisible when $\alpha = 2\pi$ (where \mathbf{g} is the reflection vector for imaging, and \mathbf{P} is the displacement vector of APB) [10]. The observation of APBs reveals the occurrence of a disorder-order transformation, which results in the formation of chemically ordered domains within the NA sample. In essence, the ordered phase domain has the same crystal structure as that of the disordered phase domain, except it takes up a superlattice

arrangement because of the periodic occupation of lattice sites by specific atom species. Accordingly, new chemically ordered α'' phase is proposed and its structure is identified by a comparison between observed and simulated diffraction patterns. The illustrations of two possible schemes for the disorder-order transformation in α'' phase are illustrated in Fig. 4. For the ordering transformation of Scheme I, U atoms occupy the following three specific lattice sites of the ordered superlattice (4 lattice sites/unit cell): $(0,5/6,1/2)$, $(1/2,1/3,1/2)$, and $(1/2,1/2,0)$, whereas the $(0,0,0)$ lattice site is randomly occupied by U and Nb atoms, in which the probability of the site occupied by U and Nb are 44% and 56%, respectively. For the ordering transformation of Scheme II, U atoms occupy $(0,5/6,1/2)$ and $(1/2,1/3,1/2)$ lattice sites, whereas the $(0,0,0)$ and $(1/2,1/2,0)$ lattice sites are randomly occupied by U and Nb atoms, in which the probability of the sites occupied by U and Nb are 72% and 28%, respectively. The systematic variations in the atomic positions result in different ordered-domains separated by APBs across which the atoms have the wrong immediate neighbors, which is illustrated in Fig. 4(a). It is also noted that the Scheme II ordering transformation as illustrated in Fig. 4(b) may also be considered as a spinodal decomposition with the wave-length (λ) of composition fluctuation that is equal to the lattice parameter of α'' unit cell in the z-direction, i.e. $\lambda = c = 0.495$ nm, which is approximately an order smaller than that observed within samples artificially aged at 200°C.

The $[110]$ -, $[310]$ -, $[312]$ -, and $[100]$ -zone selected-area diffraction patterns generated from the 15-year NA sample are shown in Figs. 5 and 6, in which the corresponding zone diffraction patterns simulated according to the Schemes I and II ordering transformations are also displayed. It is noted that the simulation patterns of the $[110]$ -, $[310]$ -, and $[312]$ -zone are identical between Scheme I and II as shown in Fig. 5, whereas the simulation patterns of the $[001]$ -zone are different between Scheme I and II as shown in Fig. 6. The ordering transformation of α'' phase is identified to be most likely of Scheme II type in accordance to the observed and simulated $[100]$ -zone patterns as shown in Fig. 6. A typical $g \cdot P$ image-contrast analysis for APBs in a 15-year NA sample is shown in Fig. 7, where the APBs are visible using $00\bar{1}$ and $0\bar{2}\bar{1}$ superlattice reflections but become invisible when using $0\bar{2}0$ fundamental reflection to image.

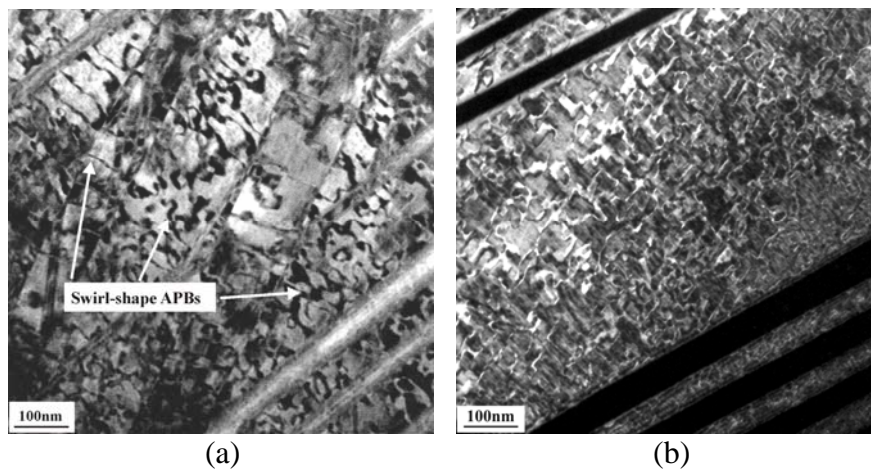


Fig. 3. Bright-field (a) and dark-field (b) TEM images reveal the formation of swirl-shape antiphase domain boundaries (APBs) within the 15-year NA sample. Notice that APBs appear as a dark contrast in (a) and a bright contrast in (b).

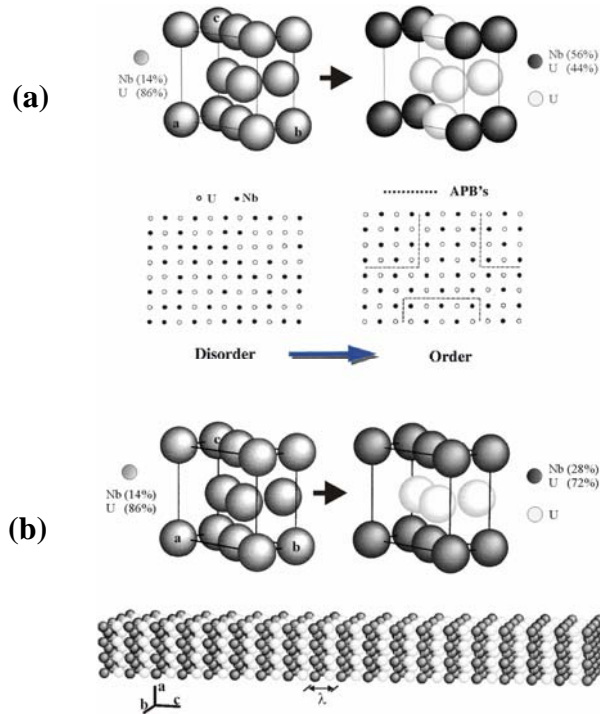


Fig. 4. Schematic illustrations showing two possible schemes proposed for the disorder-order transformation occurred in the binary U-14at%Nb (U-6wt%Nb) alloy, in which two different partially ordered α'' unit cells can be generated according to (a) Scheme I. and (b) Scheme II ordering transformations.

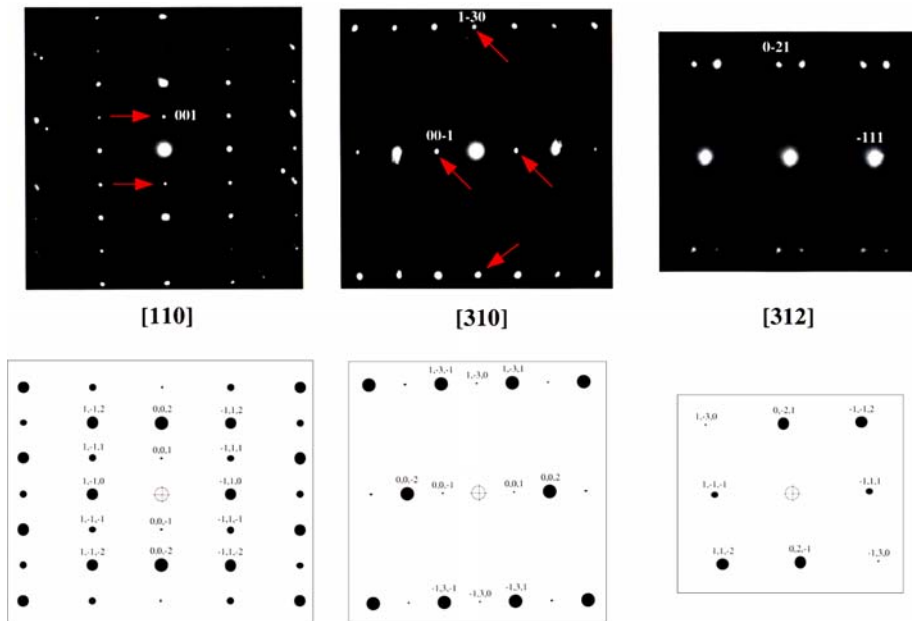


Fig. 5. The [110]-, [310]-, and [312]-zone diffraction patterns generated from the 15-year NA sample, in which the superlattice spots are arrowed (upper). Note that the [312]-zone diffraction pattern includes the diffraction spots generated from twin domains. The corresponding zone diffraction patterns simulated for the proposed ordered α'' unit cell according to Schemes I and II ordering transformations are shown below.

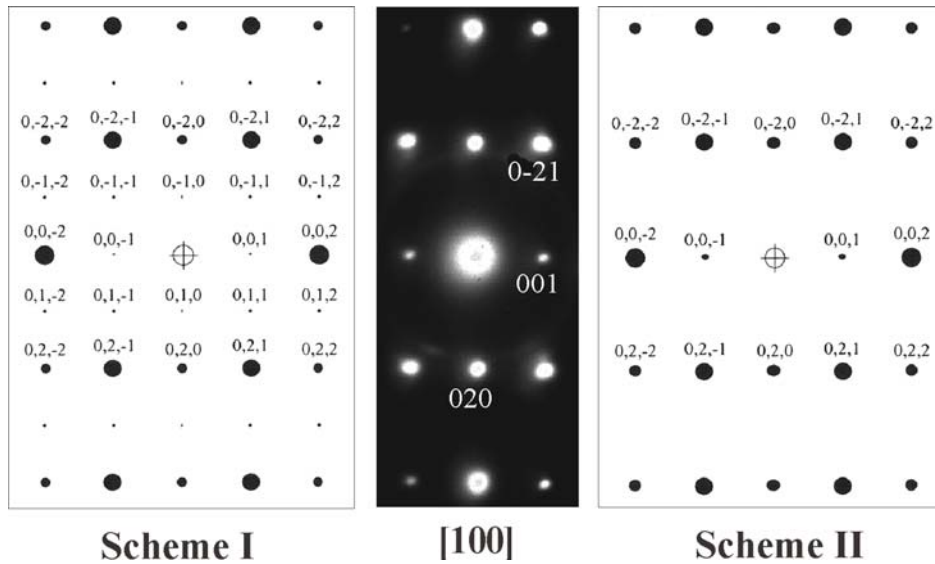


Fig. 6. The [100]-zone diffraction pattern generated from 15-yr NA sample shown with simulated patterns based upon scheme I and scheme II unit cells. Here, scheme II is more likely to be the one for the partially ordered α'' phase according to the comparison between observed and simulated patterns.

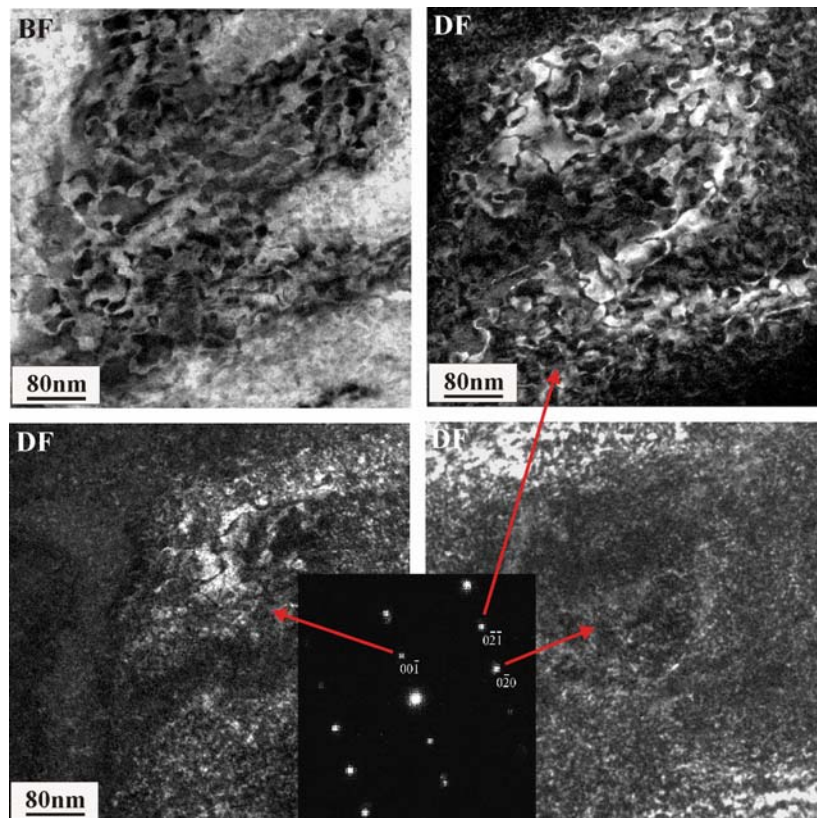


Fig. 7. BF and DF images of growth APBs in an ordered α'' domain observed in the same area. The APBs are visible using $00\bar{1}$ and $0\bar{2}\bar{1}$ superlattice reflections but become invisible when using $0\bar{2}0$ fundamental reflection to image.

Conclusion

Low-temperature aging mechanisms of a water-quenched U6Nb alloy artificially aged at 200°C for different periods of time (2, 4, 8, and 16 hours) and naturally aged at an ambient temperature for 15 years have been investigated. Age hardening/softening phenomenon is observed from the artificially aged samples. The hardness of the artificially aged alloy samples initially increases from HV 190.0 ± 5.8 (WQ) to HV 254.8 ± 12.2 (8h) and subsequently decreases to HV 237.3 ± 10.0 (16h). The hardening/softening phenomenon can be well rationalized by the occurrence of spinodal decomposition (i.e. the fine-scale of Nb segregation) within the artificially aged samples. A modulated structure (presumably containing very fine domains of Nb-lean and Nb-rich phases) is first found within α'' (monoclinic) parent phase at a very local region of the sample aged for 2 hours. The wavelength of the modulation (~3 nm) is determined according to the spacing of satellite spots exited by the [001] modulation around the Bragg peaks. The modulation becomes more pronounced after aging for 8 hours, which results in the increase of hardness to a maximum. Further aging of the alloy causes the coarsening of segregated domains and results in the decrease in hardness. The occurrence of order-disorder transformation is found within the naturally aged alloy based upon the observation of antiphase boundaries (APBs). A partially ordered α'' phase is proposed and identified based upon the comparison between observed and simulated diffraction patterns.

Acknowledgements

This work was performed under the auspices of the U. S. Department of Energy by the University of California, Lawrence Livermore National Laboratory under Contract No. W-7405-Eng-48. The authors gratefully acknowledge Bob McKoon, Anne Sunwoo, and T. C. Sun for their contribution to the heat treatment of the U6Nb alloy, Cheng Saw and Octavio Cervantes for the X-ray diffraction analysis, Bob Vallier and Vicki Mason-Reed for the microhardness measurement, and Rick Gross and Jesse Welch for the preparation of TEM foils.

References

1. Vandermeer, R.A., Acta Metall., **28** (1980), p. 383.
2. Eckelmeyer, K.H., Romig, A.D., and Weirick, L.J., Met. Trans. A, **15A** (1984), p. 1319.
3. Vandermeer, R.A., Ogle, J.C., and Northcutt, Jr., W.G., Met. Trans. A, **12A** (1981), p. 733.
4. Field R.D., Thoma D.J., Dunn, P.S., Brown D.W., Cady. C.M, Pil. Mag. A, **81** (2001), p. 1691.
5. Jackson, R.J., Miley, D. V., Trans. ASM, **61** (1968), p. 336.
6. Beverini, G., Edmonds, D.V., Colloque De Physique, Colloque **C8**, C8-429.
7. Cahn J.W., Trans. TMS of AIME, **242** (1968), p. 166.
8. Sato K.and Stobbs, W.M., Phil. Mag. A, **69** (1994), 349.
9. Butler E.P. and Thomas, G., Acta Metall., **18** (1970), 347.
10. J.W. Edington, Practical Electron Microscopy in Materials Science, Van Nostrand Reinhold, New York, 1976.